Inorganic Chemistry
Article

Inorg. Chem. **2010**, *49*, 11077–11083 **11077**
DOI: 10.1021/ic1016214

Selective Oxygen-Plasma-Etching Technique for the Formation of ZnO−FTO Heterostructure Nanotubes and Their Rectified Photocatalytic Properties

N. Chantarat,[†] Yu-Wei Chen,[†] Chin-Ching Lin,[‡] Mei-Ching Chiang,[‡] and San-Yuan Chen*[,†]

[†]*Department of Materials Science and Engineering, National Chiao Tung University, 1001 Ta-Hsueh Road, Hsinchu, Taiwan, Republic of China, and* [‡]*Materials and Chemical Research Laboratories, Industrial Technology Research Institute, Chutung, Hsinchu, Taiwan, Republic of China*

Received August 10, 2010

A novel ZnO−FTO heterostructure nanotube array was produced by combining a chemical solution process with oxygen-plasma etching. In this approach, presynthesized ZnO nanorod arrays act as templates, and FTO nanoparticles are deposited onto the ZnO nanorods by a simple spray pyrolysis method. X-ray photoelectron spectroscopy analysis demonstrated that the oxygen-plasma treatment decreased the O^{2-}/OH^{-} concentration ratio, resulting in dissociation of the Zn−O bonds and the outward diffusion of Zn cations to form an interior hollow, which is related to the formation of the hydroxyl functional group, Sn−OH, at the FTO surface. An etching evolution mechanism of the ZnO−FTO nanotubes via oxygen plasma was tentatively proposed in this study. Time-dependent photocurrent (*I*−*T*) measurements under ON−OFF cycles of UV illumination confirm that the 20-min etched sample exhibits a rectified photoresponse characteristic and a dark current increased by about 3 orders of magnitude over that of the unetched sample, which is attributed to the increased carrier concentration created at the surface conductive layer. This investigation offers an alternative selective etching method to lay the framework for nanoscale three-dimensional electrodes for solar-cell applications.

Introduction

Low-dimensional, nanostructured materials have attracted much attention for advanced electronic, optoelectronic, and photocatalytic applications because of their high sensitivity level and surface-volume characteristics. Of particular interest are coaxial nanotubes, in which core−shell hybrids are composed of oxide semiconductors, for use as three-dimensional (3D) transparent conductive (TCO) electrodes in photoelectrochemical cells.

In dye-sensitized solar cells (DSSCs), typically a TCO electrode has been used as the back contact for the nanostructured TiO_2 film. In particular, heterostructured, one-dimensional (1D) electrodes have received great attention because of their chemically oxidative and hybrid properties, which were proposed to improve the conversion efficiency as an alternative approach to DSSCs.[1−4] Recently, Wang et al. demonstrated that the photoelectric conversion efficiency of the DSSCs made from an indium−tin oxide (ITO) nanowire array embedded with the TiO_2 photoelectrode was higher than that of a pristine TiO_2 film or arrays of ITO/TiO_2 core−shell nanowires.[1] Liao and co-workers reported hybrid CdS/P3HT photovoltaic devices using FTO-coated ZnO nanorod (NR) arrays as 3D electrodes. The FTO-coated ZnO NR length and thickness of the FTO layer were interpreted to enhance the photovoltaic performance.[2]

Generally, the unique properties of ZnO are utilized not only in various aligned nanostructures for charge-carrier transportation and light emission but also as a free-standing NR, which is suited for uniformly nanosized templates and can be functionalized via interfacial solid-state diffusion with a surrounding shell layer. As a shell layer, the transparent conducting FTO is thought to be an ideal candidate electrode for solar cells. In addition, it was well-known that a high aspect ratio of 1D FTO nanostructures can provide far greater surface area than thin films, offering the additional challenge of obtaining effective charge-carrier collection and transport. Therefore, if the ZnO-embedded FTO could put forward the idea of extension into nanotubes with a completely hollow core, the large interfacial area between FTO and ZnO will play a critical role in improving the conduction path through nanoscale effects.[5] However, there have not been any reports involving the fabrication of a ZnO/FTO

*To whom correspondence should be addressed. E-mail: sanyuanchen@mail.nctu.edu.tw. Tel: +886-3-5731818. Fax: +886-3-5725490.

(1) Wang, H. W.; Ting, C. F.; Hung, M. K.; Chiou, C. H.; Liu, Y. L.; Liu, Z. W.; Ratinac, K. R.; Ringer, S. P. *Nanotechnology* **2009**, *20*, 055601.
(2) Liao, H. C.; Lin, C. C.; Chen, Y. W.; Liu, T. C.; Chen, S. Y. *J. Mater. Chem.* **2010**, *20*, 5429–5435.
(3) Joanni, E.; Savu, R.; Góes, M. D. S.; Bueno, P. R.; Freitas, J. N. D.; Nogueira, A. F.; Longo, E.; Varela, J. A. *Scr. Mater.* **2007**, *57*, 277–280.
(4) Yuhas, B. D.; Yang, P. *J. Am. Chem. Soc.* **2009**, *131*, 3756–3761.
(5) Zheng, L.; Zheng, Y.; Chen, C.; Zhan, Y.; Lin, X.; Zheng, Q.; Wei, K.; Zhu, J. *Inorg. Chem.* **2009**, *48*, 1819–1825.

Published on Web 11/10/2010

hollow nanotube and related optoelectronic properties. Therefore, when ZnO as the active light-absorbing component is combined with oriented FTO nanotube arrays, this composite nanostructure possesses excellent charge-transport characteristics, which will be a benefit for photovoltaic devices.

To the present, there have been a number of reports on template-assisted oxide nanotube formation by various synthesis methods. Selective etching is one important technique to produce controllable structures, including wet-chemical etching[6−10] and hydrothermal treatment.[11−15] Zeng et al. developed wet-etched Zn−ZnO core−shell nanoparticles (NPs), where H^+ ions incorporated from a weak acid solution diffused along lattice defects and grain boundaries in the ZnO shell layer to eliminate Zn core materials via a redox-precipitation process at the interface.[8] Fan et al. developed $ZnAl_2O_4$ nanotube structures using hydrothermal calcination. The formation mechanism includes the occurrence of defects and voids along the core−shell interface, and the Kirkendall effect with surface diffusion produces hollow interiors.[12] Yao et al. proposed a two-step etching process on ZnO NRs, which entails both chemical and plasma etching at low temperature.[15] A wet acid solution provides a rough isotropic etch of hexagonal edges, and then argon plasma is employed to fabricate controllable nanotips for enhanced field-emission devices. However, the wet-etching process leads to a morphology with a high degree of disorder, causing a lower photocatalytic efficiency due to photocorrosion. Therefore, it is very important to develop a dry-etching synthesis process for the metal oxide semiconductor in solar cell applications. To date, there has been little research on dry-etching mechanisms, in which a controllable etching rate could improve the optical properties of the materials. The use of oxygen plasma to eliminate the inner core of metal oxide compounds has only been studied in a few cases, but this novel method could introduce the benefits of hollow nanoscale materials.

In this paper, we propose a fabrication method to synthesize ZnO−FTO composite nanotubes using water-based spray pyrolysis for depositing FTO NPs on arrayed ZnO NRs and oxygen plasma for the etching process. During the process, various ions and radicals generated by the oxygen plasma, including O^+, O^{2+}, and O*, can readily diffuse into oxygen vacancies[16−18] to create negative charges on the ZnO NR surface. This results in an accelerated etching rate, producing a large number of voids in ZnO and forming a hollow ZnO−FTO heterostructure. The mechanism of etching evolution of the ZnO−FTO nanotubes via oxygen plasma was also investigated in this study. In addition, the corresponding enhanced photoresponse of the heterostructures will also be discussed.

Experimental Procedure

ZnO NRs were grown on a ZnO-film-coated glass substrate by an aqueous mixture of zinc nitrate hexahydrate [$Zn(NO_3)_2 \cdot 6H_2O$] and hexamethylenetetramine in deionized water with ratios of 1:1. Prior to the actual concentration, each sample was kept in an electric oven at 85 °C for 10 h of wet-chemical growth. After synthesis, the ZnO products were rinsed several times with deionized water and dried in air. To explore the potency of our new strategy, we synthesized the highly ordered template-based ZnO−FTO core−shell structure. The depositing precursors of FTO films were synthesized from $SnCl_2 \cdot 4H_2O$ dissolved in deionized water and stirred vigorously for 30 min. In order to obtain well solubility, 5% HCl was added into the precursor solution. Upon stirring, the solution immediately became transparent, indicating its purification. Finally, a 50% NH_4F precursor was added at room temperature and kept stirring for 5 min. Depositions were carried out in an ultrasonic neubilizer reactor, of which the temperature was constantly kept at 380 °C to spontaneously deposit the small NPs on the ZnO NR arrays to form FTO film/ZnO NR composite nanostructures. After deposition of the FTO layer, we observed that the color of the samples turned from white to yellowish because of the high substrate temperature.

Subsequently, the samples were treated by oxygen plasma [P = 350 mTorr and radio-frequency (RF) power = 350 W] for 0, 2, 10, and 20 min. After treatment, the morphology of ZnO NRs and the ZnO−FTO heterostructure under the progress of oxygen plasma was investigated by a scanning electron microscope (JEOL JSM-6700F) and a high-resolution transmission electron microscope (JEOL 2100) operated at 200 keV. To analyze the oxygen incorporation into the ZnO layer after deposition of FTO, photoluminiescence (PL) measurements were carried out with a He−Cd laser (365 nm) as the excitation source at room temperature. The structural evolution was also characterized by X-ray diffraction (XRD) and X-ray photoelectron spectroscopy (XPS). Photon absorbance was measured by $I-T$ measurement of the UV light source (λ = 365 nm) using a model 600C series electrochemical analyzer with an applied direct-current voltage of +5 eV, and ON−OFF cycles were consistently repeated within a 1600-s time trace.

Results and Discussion

Figure 1a is a high-magnification scanning electron microscopy (SEM) image showing the ZnO NR array structures, with NR lengths ranging from a few tens to hundreds of micrometers and diameters between 50 and 100 nm. After FTO coating, the ZnO NRs become larger in diameter because of the additional rough FTO layer covering the entire ZnO NR, as shown in Figure 1b. Figure 2 shows high-resolution transmission electron microscopy (HRTEM) images of a core−shell ZnO−FTO heterostructure (a) before and (b) after exposure to oxygen plasma for 20 min at room temperature. The low-magnification image in the inset of Figure 2a illustrates that the FTO monolayer has uniformly covered the ZnO NRs to form a ZnO−FTO core−shell structure. The HRTEM images magnified from the red rectangle in the inset of Figure 2a further demonstrate that the FTO layer on the ZnO NRs is composed of FTO NPs,

(6) Zeng, H. C. *J. Mater. Chem.* **2006**, *16*, 649–662.
(7) Kuang, Q.; Jiang, Z. Y.; Lin, S. C.; Lin, Z. W.; Xie, S. Y.; Huang, R. B.; Zheng, L. S. *J. Am. Chem. Soc.* **2005**, *127*, 11777–11784.
(8) Zeng, H.; Cai, W.; Liu, P.; Xu, X.; Zhou, H.; Kling, C.; Kalt, H. *ACS Nano* **2008**, *2*, 1661–1670.
(9) An, K.; Kwon, S. G.; Park, M.; Na, H. B.; Baik, S. I.; Yu, J. H.; Kim, D.; Son, J. S.; Kim, Y. W.; Song, I. C.; Moon, W. K.; Park, H. M.; Hyeon, T. *Nano Lett.* **2008**, *8*, 4252–4258.
(10) Liu, B.; Zeng, H. C. *J. Phys. Chem. B* **2004**, *108*, 5867–5874.
(11) Liu, B.; Zeng, H. C. *J. Am. Chem. Soc.* **2004**, *126*, 16744–16746.
(12) Fan, H. J.; Knez, M.; Scholz, R.; Hesse, D.; Nielsch, K.; Zacharials, M.; Gösele, U. *Nano Lett.* **2007**, *7*, 993–997.
(13) Zeng, H.; Li, Z.; Cai, W.; Cao, B.; Liu, P.; Yang, S. *J. Phys. Chem. B* **2007**, *111*, 14311–14317.
(14) Yang, Y.; Kim, D. S.; Scholz, R.; Knez, M.; Seung, M. L.; Gösele, U.; Zacharias, M. *Chem. Mater.* **2008**, *20*, 3487–3494.
(15) Yao, I. C.; Lin, P.; Tseng, T. Y. *Nanotechnology* **2009**, *20*, 125202.
(16) Chen, Y.; Bagnall, D. M.; Koh, H. J.; Park, K. T.; Hiraga, K.; Zhu, Z.; Yao, T. *J. Appl. Phys.* **1998**, *84*, 3912–3918.
(17) Wolden, C. A. *Plasma Chem. Plasma Process.* **2004**, *25*, 169–192.
(18) Liu, M.; Kim, H. K. *Appl. Phys. Lett.* **2004**, *84*, 173–175.

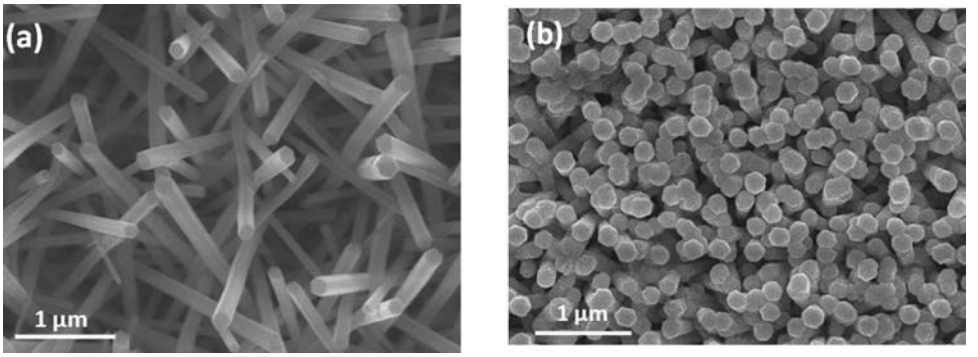

Figure 1. Field-emission SEM images of (a) as-deposited ZnO NRs grown on a Corning glass substrate using a hydrothermal method and (b) FTO coating on ZnO NRs obtained by spray pyrolysis deposition. The FTO deposition time was 2 min at 380 °C.

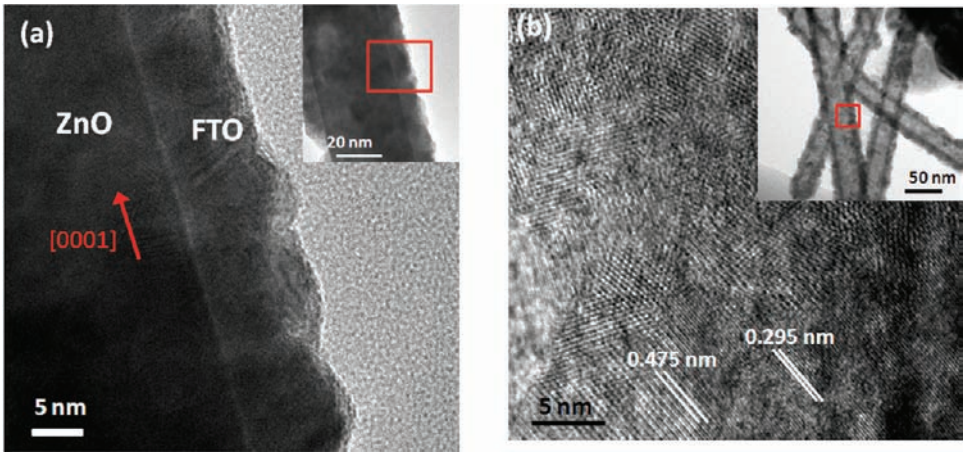

Figure 2. HRTEM images of core−shell ZnO−FTO heterostructures (a) before and (b) after exposure to oxygen plasma for 20 min at room temperature, The insets of parts a and b show the magnified interface, indicated by the red rectangle.

with a wall thickness of about 15 nm. On the other hand, for ZnO−FTO composites treated with dry oxygen plasma, the ZnO NR core was removed to form a 1D tubelike FTO nanostructure, as shown in the inset of Figure 2b. This occurs because the wurtzite ZnO NR template can be more rapidly etched along the [0001] direction compared with the tetragonal rutile FTO. The HRTEM image in Figure 2b reveals that the ZnO−FTO composite nanotube contains ZnO-{0001} and FTO-{100} planes, with the lattice spacing of certain atomic planes at about 0.475 and 0.295 nm, respectively. Consequently, it can be assumed that some residual ultrafine ZnO nanocrystals have been embedded into the surface of the FTO shell layer after the etching process through an interfacial solid-state reaction between ZnO and FTO.[7,12,14]

The cross-sectional images, analyzed by transmission electron microscopy (TEM)−energy-dispersive spectrometry (EDS) line scans across the tube diameter (side view, Figure 3a,b; top view, Figure 3c,d), show hollowlike regions, which clearly indicate a ZnO−FTO heterogeneous nanotube. The EDS elemental line scans on the ZnO−FTO samples indicate that, after dry etching, the heterogeneous structure is mostly composed of Sn, with residual ZnO isotropically distributed either alongside or in the interior of the FTO tube wall. In particular, the relative composition ratios of the elements Sn, Zn, and O were estimated as about 4.5:1:3.5 (side view) and 7:1:6 (top view), respectively. As a result, the relative ratio of Sn to Zn in Figure 3d is apparently larger than that in Figure 3b, further confirming that the ZnO region in the core has been etched successfully.

The relative removal of the inner core using the oxygen-plasma treatment under RF power (350 W, at room temperature) with etching time was also observed. The TEM images in Figure 4a−c show the structural evolution of the inner ZnO core corresponding to different treatment durations (0, 2, and 20 min, respectively). The TEM image in Figure 4a shows an interfacial gap after spray coating of the FTO onto the ZnO NRs between the FTO layer and ZnO, caused by the lattice mismatch between the two. Oxygen-plasma etching for 2 min can lead to a polycrystalline ZnO sheath with formation and enlargement of the voids along the ZnO−FTO interface, as indicated in Figure 4b, suggesting that the voids were possibly initiated from the mismatch sites between the FTO layer and ZnO. With increased reaction time (20 min), it can be seen in Figure 4c that the inner ZnO core was almost consumed and the hollow formation took place along the [0001] plane to form a nanotubelike structure. The XRD pattern in Figure 5 shows the characteristic peaks of a ZnO−FTO core−shell structure as a function of the etching time. As-grown ZnO NRs mainly display oriented peaks in the descending order of (100), (002), (101), and (110), and as-deposited ZnO−FTO shows the additional FTO peaks to the ZnO peaks. After treatment with the oxygen plasma for 2 min, the relative peak intensity of ZnO was reduced, although the (100) peak can still be observed.

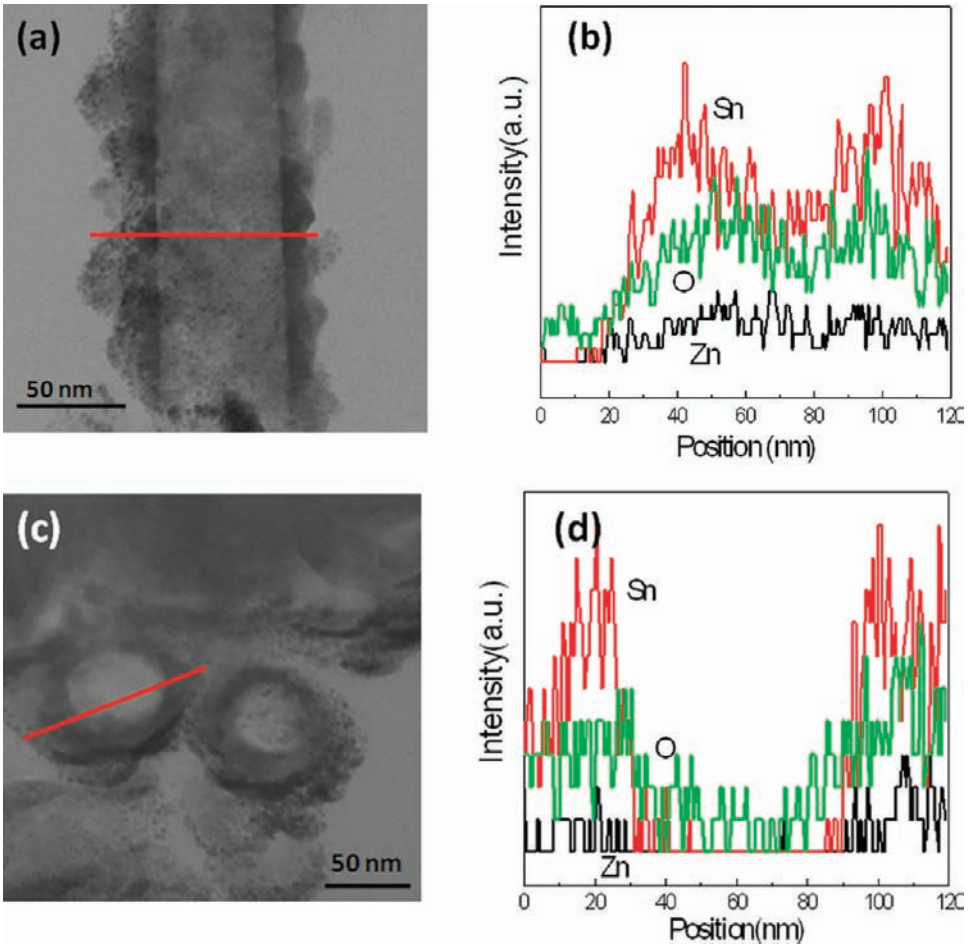

Figure 3. Cross-sectional HRTEM and EDS line scans of an ZnO−FTO nanotube fabricated by dry oxygen-plasma etching at 20 min: (a and b) side view; (c and d) top view.

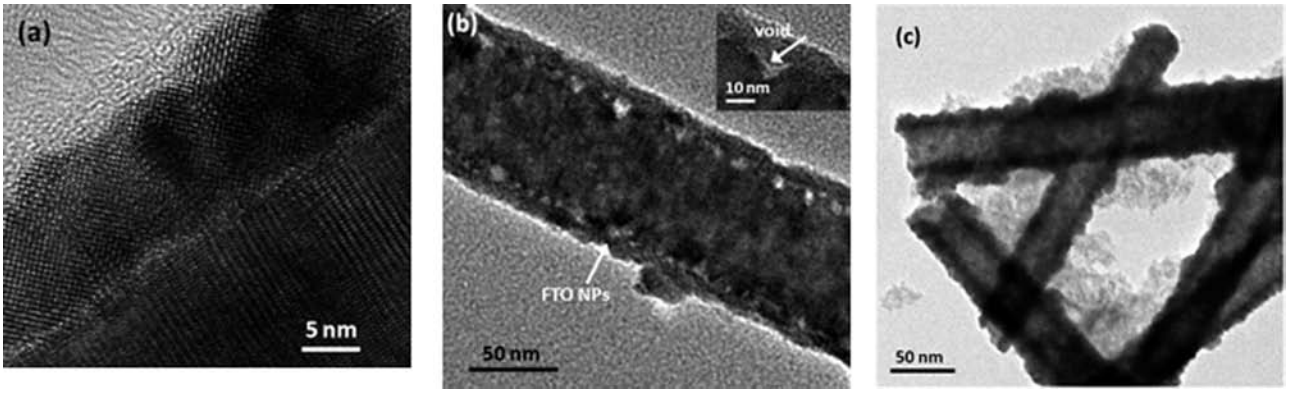

Figure 4. Formation of voids in the FTO-coated ZnO obtained before and after etching of ZnO NRs as a function of time: (a) 0 min; (b) 2 min; (c) 20 min. The inset of part b is a high-resolution image of the void.

A long oxygen-plasma treatment time of 20 min resulted in a further reduction in the ZnO peak intensity so that it became negligible. Thus, the XRD peaks of the ZnO−FTO tubelike heterostructures display differences from the as-deposited ZnO−FTO. This indicates that the ions and radicals from the oxygen plasma indeed impart an impact energy to the ZnO NRs to induce different degrees of etching, which cause a morphological transformation. The impact energy from the oxygen plasma is high enough to induce transformation and dissociation of ZnO, suggesting that more excess vacancies could be generated and accumulated at the interfaces. This suggestion is confirmed by PL, which will be discussed later.

Figure 6 shows room-temperature PL spectra using 365-nm UV excitation for ZnO and ZnO−FTO treated with oxygen plasma for 0, 2, 10, and 20 min. Two main bands were obtained: the strong peak in the UV emission spectrum at 380 nm corresponds to the near band edge (I_{NBE}) generated by the recombination of free electrons and a broad-band visible deep-level emission (I_{DLE}) centered at ~600 nm induced by impurities and defects such as oxygen vacancies (V_O^+) and

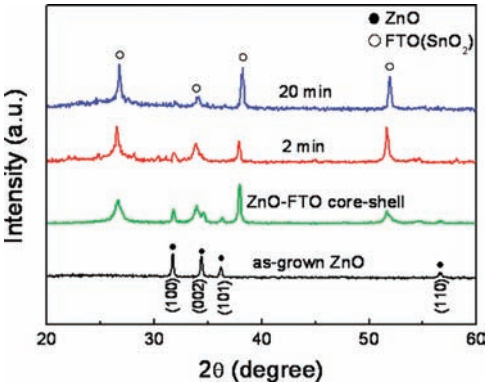

Figure 5. XRD patterns of as-grown ZnO and ZnO−FTO heterostructures on glass treated for the times noted under oxygen plasma. The patterns are vertically offset for clarity.

zinc interstitials (Zn_i).[19−21] It was found that with, a plasma-treatment duration of 2 min, well-aligned ZnO NRs with well-defined hexagonal planes remained unchanged. However, under a longer plasma duration, such as 10 min, the pristine ZnO NR displayed a relatively enhanced defect density, which caused a decreased I_{NBE} and an increased I_{DLE}, as expected (Figure 6a). These results are probably related to deterioration of the ZnO NRs, as seen in the inset of Figure 6a. On the other hand, after FTO coating, it was observed that I_{NBE} from ZnO was enhanced compared to the pristine ZnO because of defect passivation. However, with a plasma etching time of 2 min, Figure 6b shows a significant reduction in I_{NBE} but only a slight reduction in I_{DLE}. After plasma treatment (> 2 min), it was found that both peaks were reduced to a negligible height, indicating that ZnO could be etched after FTO coating using a longer oxygen-plasma treatment. This reveals that the FTO shell can not only passivate the surface defects on the ZnO NRs to enhance I_{NBE} but also trigger the ZnO etching of the ZnO−FTO nanocomposite to produce the ZnO−FTO nanotube heterostructure. All of the evidence confirms that the FTO layer plays a key role as a gas-nanocatalytic absorber[22−25] to enhance the etching activity on the ZnO template.

It was assumed that the phase transformation of ZnO solid to Zn vapor was initiated by the sprayed FTO NPs and the oxygen-plasma treatment at the ZnO−FTO interface. Later, it was found that, with a prolonged oxygen-plasma treatment (> 2 min), ZnO in the interior was continuously etched, along with void formation and phase transformation of ZnO solid into Zn vapor, which induced the defect diffusion outward from the core layer and promoted the formation of a tubelike structure.

To further understand the possible oxygen-plasma-etching mechanism, XPS was performed on the samples. Parts a and b of Figure 7 show the XPS spectra of the O 1s peak in the as-synthesized FTO-coated ZnO samples without and with a preheat treatment, respectively. It shows a correspondence to the binding energy of the occurrence of two deconvoluted components: formation of the hydroxyl (OH) functional group at 532.89 eV may be generated during hydrothermal growth or wet-solution-based synthesis and the O^{2-} ions bonded in the lattice (Zn−O and Sn−O) as identified at 531.32 eV. However, the hydroxyl peak is negligible compared to the O^{2-} peak.

After exposure of the samples to a 350-W oxygen plasma for 20 min (Figure 7c), it is apparent that the plasma treatment caused a decrease in the number of the O^{2-}/OH^- concentration ratio, as compared to samples that did not undergo the plasma process (Figure 7a). More specifically, it is implied that the OH^- ion, produced by the oxygen plasma, is initially physisorbed onto the FTO surface. The hydroxylated FTO substrate is then constructed in the form of Sn−OH at the outermost surface via oxidation and nucleophilic attack of H_2O molecules in the atmosphere. For the reaction under ambient conditions, the active species in the oxygen plasma (OH^-) also induces the accumulation of hydroxyl radicals (•OH) at the FTO surface because of a primary photocatalytic effect, for which the radicals in the gas phase could be generated and diffused toward FTO, interfacial ZnO−FTO, and the ZnO layer, respectively. Thus, the dissociation of Zn−O bonds can be caused by the impact of •OH radicals from the physical bombardment of oxygen molecules and the shift of the cationic zinc species away from the core center. Meanwhile, oxygen plasma could also introduce defects (oxygen vacancies) into the FTO surface. If FTO has defects, the oxygen-plasma incorporation might result in a reduction of the O^{2-} concentration from Sn^{4+}−O (FTO). Thus, the existence of Sn^{2+}−O bonds (tin monoxide, SnO) could be observed[26,27] and confirmed as the contribution of O−Sn−OH, meaning that the native oxide layer was eliminated from the depletion region at the surface, as demonstrated in Scheme 1. Furthermore, the binding energy of 534.55 eV was assigned to the generation of molecular oxide and tin bonding (O_2^{2-}), which is known to be the most stable plasma species generated by the excited molecular oxygen in the plasma. Nagasawa et al.[27] reported that an increased density of this absorbed oxygen species on the surface is correlated to the existence of O_2^{2-} ions at Sn^{2+} sites, which is responsible for a reduction of O^{2-} (or the generation of Sn^{4+}−O), as mentioned above.

In addition, the sample with a preheat treatment at 500 °C before the plasma process was also tested in the same way as nonpreheated samples for comparison. As a result, there is no big difference between parts a and b of Figure 7, confirming that 500 °C is not hot enough for sufficient thermal agitation to deteriorate the ZnO bond strength and to produce the hollow interiors. On the other hand, the reduction of the O^{2-} intensity (Zn−O bonds) in Figure 7d as compared to Figure 7b is again dominated by plasma treatment, showing behavior similar to that of nonpreheated samples. Moreover, the relative intensity ratios of O^{2-}/OH^- (2.63) and O_2^{2-}/OH^- (1.28) in Figure 7d are slightly lower than those in Figure 7c (3.16 and 1.62, respectively) because of an increase

(19) Cheng, H. M.; Lin, K. F.; Hsu, H. C.; Hsieh, W. F. *Appl. Phys. Lett.* **2006**, *88*, 261909.
(20) Yang, Y. H.; Chen, X. Y.; Feng, Y.; Yang, G. W. *Nano Lett.* **2007**, *7*, 3879–3883.
(21) Hsiao, C. S.; Chen, S. Y.; Kuo, W. L.; Lin, C. C.; Cheng, S. Y. *Nanotechnology* **2008**, *19*, 405608.
(22) Xue, X. Y.; Chen, Y. J.; Liu, Y. G.; Shi, S. L.; Wang, Y. G.; Wang, T. H. *Appl. Phys. Lett.* **2006**, *88*, 201907.
(23) Zhang, Y.; Kolmakov, A.; Chretien, S.; Metiu, H.; Moskovits, M. *Nano Lett.* **2004**, *4*, 403–407.
(24) Kim, K. W.; Cho, P. S.; Kim, S. J.; Lee, J. H.; Kang, C. Y.; Kim, J. S.; Yoon, S. J. *Sens. Actuators B* **2007**, *123*, 318–324.
(25) Choi, S. W.; Park, J. Y.; Kim, S. S. *Nanotechnology* **2009**, *20*, 465603.
(26) Nagata, T.; Bierwagen, O.; White, M. E.; Tsai, M. Y.; Speck, J. S. *J. Appl. Phys.* **2010**, *107*, 033707.
(27) Nagasawa, Y.; Choso, T.; Karasuda, T.; Shimomura, S.; Ouyang, F.; Tabata, K.; Yamaguchi, Y. *Surf. Sci.* **1999**, *226*, 433–435.

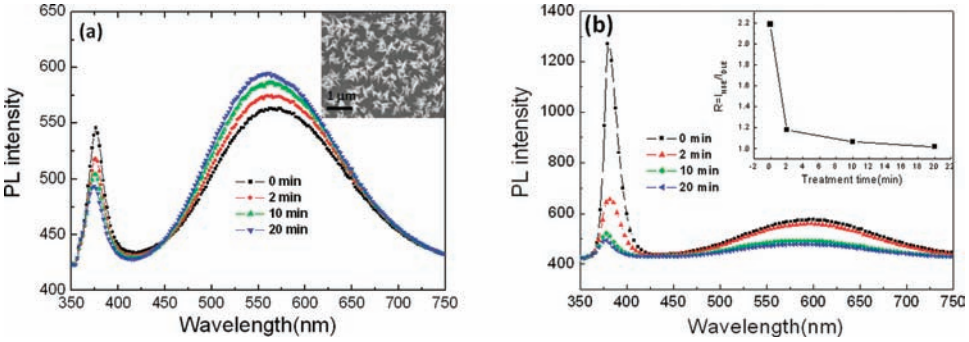

Figure 6. PL of (a) as-grown ZnO and (b) FTO-coated ZnO samples showing variation of the spectrum intensity corresponding with the plasma exposure time. The insets of parts a and b demonstrate the morphology of the ZnO NRs after 20 min of etching and the relative intensity (R) of part b, respectively.

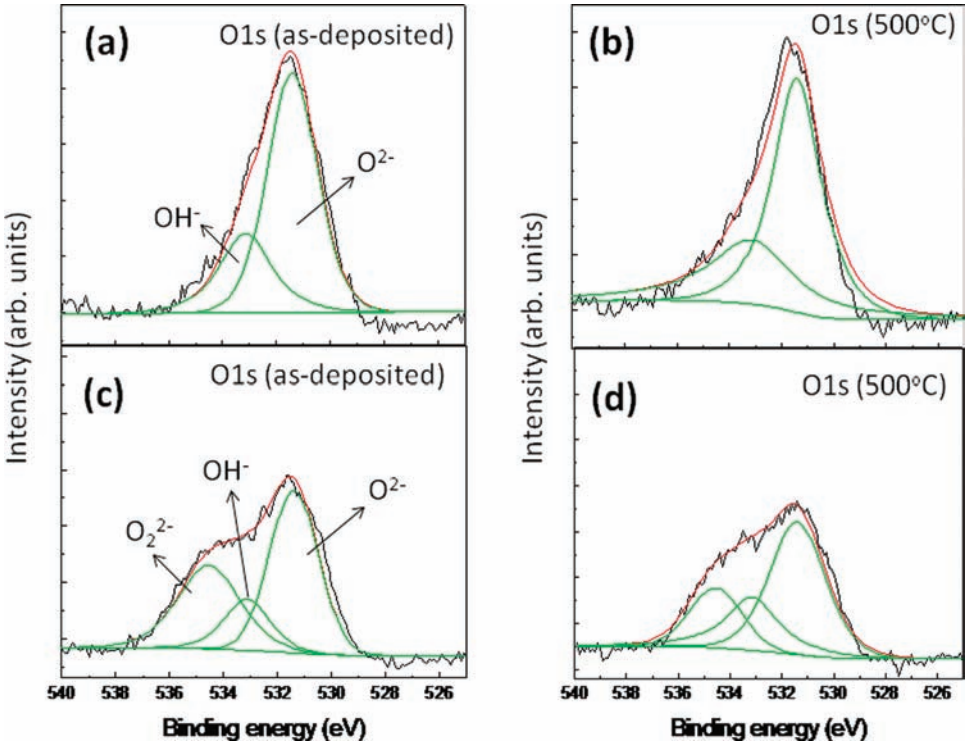

Figure 7. XPS spectra of the O 1s peak in FTO-coating ZnO samples: (a and b) before and (c and d) after plasma etching (350-W RF power for 20 min), preparing the samples with and without preheat annealing at 500 °C, as indicated in each figure.

of the OH^- density. This suggests that, although preheating can induce the activation energy of the oxygen-plasma effect to accelerate the surface diffusion of oxygen vacancies and cause somewhat of a change to the relative intensity, as compared to plasma treatment, it represents a minor effect on the etching mechanism.

Considering that the radical species can be produced via the reaction $O_2 + e^- \xrightarrow{\text{ionization}} O_2^+ + 2e^- \xrightarrow{\text{radicalformation}} 2O + e^-$ during the plasma process, high energy or heat can be generated at the surface because of ion collisions. Thus, the influx of $\bullet O^{2-}$ or $\bullet OH$ radicals can disintegrate the ZnO core to form Zn-rich regions, and the chemical reaction could even be enhanced with the released oxygen ions (O^- and O^{2-}) from the FTO layer when the oxygen molecules are absorbed on its surface, as illustrated in Scheme 1. As a result, a nonequilibrium pressure-induced stress (σ) across the interface is caused by Zn generation. Furthermore, because the melting point of Zn metal is low (about 420 °C), a higher Zn concentration can form and gasify inside the core, in which the stress was developed during the continuous reaction. The subsequent relaxation of the stress, accompanied by a decrease of energy in the core, could occur, so that the surface diffusion of metal cations (Zn) flowed outward to reach an equilibrium state and, therefore, excessive voids (hollow area) were left inside the core, whereas unconsumed ZnO NPs may be embedded near the FTO shell.[12,28]

To further illustrate the correlation between the optical and electrical properties and the etching mechanism, the sequential reduction of I_{NBE} corresponding to the PL spectra in Figure 6b was again examined in terms of photoresponse as a function of time (Figure 8a). It is known that the spectral response in ZnO NRs indeed has a cutoff wavelength of ~375 nm, whereas FTO cannot be induced to fluoresce by the long-wavelength

(28) Zhdanov, V. P.; Kasemo, B. *Nano Lett.* **2009**, *9*, 2172–2176.

Scheme 1. Top-View Cross-Sectional Schematic Diagram of an FTO-Coated ZnO Core−Shell Nanostructure, Illustrating the Oxygen-Plasma-Enhanced Etching Evolution of the ZnO−FTO Nanotube[a]

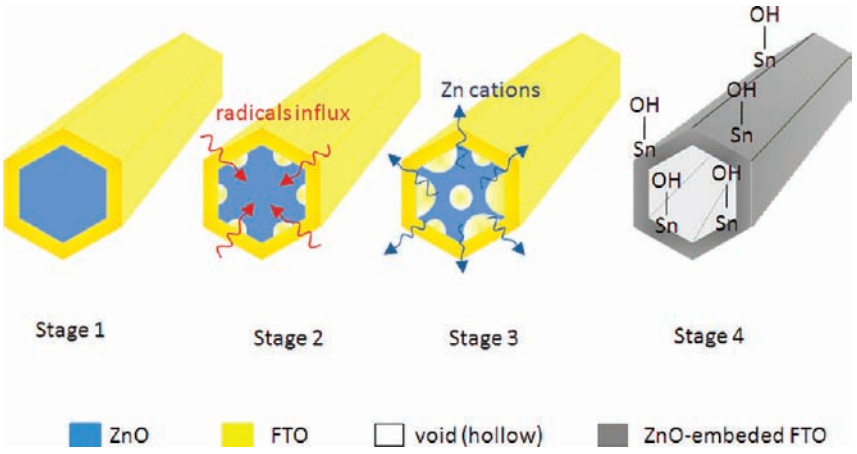

[a] The direction of outward diffusion is indicated by the arrow in stage 3.

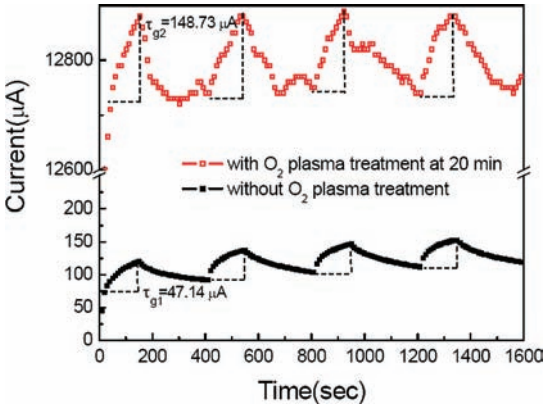

Figure 8. Under UV illumination (λ = 365 nm), with an applied voltage of +5 eV (electron conduction), τ_{g1} and τ_{g2} are shown indicating the response times of time-dependent photocurrent with (20 min) and without oxygen-plasma treatment, respectively.

UV light source, as was expected from its wide band gap (E_g = 3.6 eV). Thus, under UV illumination (λ = 365 nm) in ambient air, the ZnO−FTO samples that were plasma-etched for 20 min exhibited nonunity photoresponse exponentials. This confirms that the discontinuous surface of the etched ZnO core may influence the photon-trapping electron-transfer effects.

Despite the above discussion, the present results demonstrate that the ZnO−FTO etched for 20 min displayed an enhancement in sensitivity of about 3 orders of magnitude ($\tau_{g2} > \tau_{g1}$) and a remarkably increased dark current, from 4.539×10^{-5} to 1.234×10^{-2} A, compared to the unetched sample. On the basis of this result, it was concluded that (1) the accumulation of ZnO NPs embedded in the FTO layer still allows for excellent photon-absorbing properties and serves as a rectifying interfacial ZnO−FTO heterojunction, which can improve the separation of the electron−hole pairs and photosensitivity through discharge of the absorbed oxygen ions [$h^+ + O_2^-(ad) \rightarrow O_2(g)$], (2) the oxygen plasma can introduce a high OH^- concentration, resulting in not only an increased carrier concentration but also the negative charge of two extra electrons released from the dangling Sn^{2+}−O bonds, which can act as a donor in the Sn^{4+} matrix, creating surface charges in the host lattice of ZnO and FTO,[29] and (3) eventually the elimination of the resistive ZnO core after etching may regulate charge transport in the FTO conductive layer. Therefore, we believe that this novel structural characteristic, with an enlarged interfacial area, will offer the major advantage of using 3D ZnO−FTO tubelike electrodes for nanoarchitectural optoelectronic devices.

Conclusion

In summary, we fabricated ZnO−FTO heterostructure nanotube arrays using presynthesized ZnO NR arrays as templates and deposited FTO NPs. After undergoing a dry-oxygen plasma treatment, the formation of voids in the ZnO core was initially observed alongside the ZnO−FTO interface at 2 min, and an increased etching time created a hollow along the [0001] plane in the ZnO inner core. The XPS study indicates that degradation of the O^{2-} peak intensity (531.32 eV) can be induced by the reactive $\bullet O^{2-}$ and •OH radicals and O-ion bombardment, which corresponds to dissociation of the Zn−O bonds and the outward diffusion of Zn cations, resulting in the occurrence of the hollow interior. In addition, the time dependence of the photocurrent (I−T) under UV illumination (λ = 365 nm) shows a rectified photoresponse characteristic for the 20-min etched sample, and the dark current of this sample increases from 4.539×10^{-5} to 1.234×10^{-2} A (~3 orders of magnitude) compared to that of the unetched sample. This study demonstrates that a new architectural design with a large surface area can be further developed into a highly conductive 3D electrode with rectified photocatalytic activity for photovoltaic solar cells.

Acknowledgment. The authors gratefully acknowledge the National Science Council of the Republic of China for its financial support through Contract NSC98-3114-E-009-006.

(29) Angadi, B.; Park, H. C.; Choi, H. W.; Choi, J. W.; Choi, W. K. *J. Phys. D: Appl. Phys.* **2007**, *40*, 1422–1425.